Zigzag Inversion Domain Boundaries in Indium Zinc Oxide-Based Nanowires: Structure and Formation

Anna P. Goldstein,[†] Sean C. Andrews,[†] Robert F. Berger,[‡] Velimir R. Radmilovic,[‡,§] Jeffrey B. Neaton,[‡] and Peidong Yang[†,‡,∥,*]

[†]Department of Chemistry and [∥]Department of Materials Science and Engineering, University of California, Berkeley, Berkeley, California 94720, United States, [‡]Materials Sciences Division, Lawrence Berkeley National Laboratory, Berkeley, California 94720, United States, and [§]Faculty of Technology and Metallurgy, Nanotechnology and Functional Materials Center, University of Belgrade, 11120 Belgrade, Serbia

ABSTRACT Existing models for the crystal structure of indium zinc oxide (IZO) and indium iron zinc oxide (IFZO) conflict with electron microscopy data. We propose a model based on imaging and spectroscopy of IZO and IFZO nanowires and verify it using density functional theory. The model features a $\{\bar{1}2\bar{1}/\}$ "zigzag" layer, which is an inversion domain boundary containing 5-coordinate indium and/or iron atoms. Higher $/$ values are observed for greater proportion of iron. We suggest a mechanism of formation in which the basal inclusion and the zigzag diffuse inward together from the surface of the nanowire.

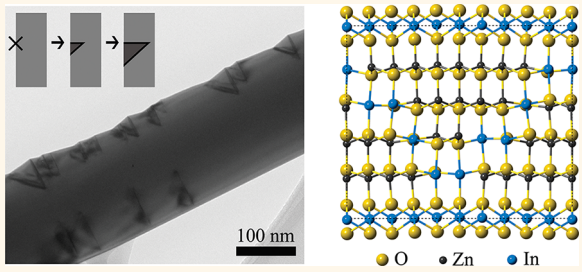

KEYWORDS: nanowires · EELS · crystal structure · zinc oxide · indium diffusion

Transparent conducting oxide (TCO) materials have attracted much interest in the electronics industry for their importance in touch-sensitive or photoactive devices. In particular, alloys of indium and zinc oxide (indium zinc oxide, or IZO) have shown significantly enhanced electron conductivity and mobility over zinc oxide.[1−3] Crystalline IZO has a remarkable structure that has generated significant interest in the 25 years since its discovery. Annealing a mixture of the precursor oxide powders (ZnO and In_2O_3) for several days at or above 1100 °C produces thin, regularly spaced layers of dark contrast visible by transmission electron microscopy (TEM).[4] The known range of materials with this structure has grown to include combinations of other trivalent metals, such as In, Fe, Ga, or Al (hereafter referred to as M). To increase the utility of IZO and related materials, their structure and formation mechanism must be more thoroughly understood.

Here we present a new model that resolves the structure of IZO and IFZO. This model is supported both by high-resolution electron microscopy and DFT calculations. A defining feature is the inversion of the metal and oxygen positions across a zigzag region, facilitated by 5-coordinate indium or iron atoms. These regions of inversion align themselves along a particular plane, depending on the local metal composition. This model accounts for our experimental observations and resolves the discrepancies between previous models. The present model also suggests that the zigzag plays a role in the formation mechanism of IZO and IFZO from the native oxides.

Previously, Cannard and Tilley observed that the IZO structure was composed of thick regions of ZnO separated by very thin In-rich layers parallel to the (0002) basal plane.[4] Kimizuka *et al.* later showed that similar layers form when equal amounts of In_2O_3 and Fe_2O_3 were annealed with ZnO to form $InFeO_3(ZnO)_n$.[5] The structure of the basal inclusions was identified as a single atomic layer of edge-sharing MO_6 octahedra with an overall formula of MO_2^-, separated from the other octahedral layers by $n + 1$ units of ZnO.[5,6] Each oxygen atom in these octahedra is tetrahedrally coordinated by three M^{3+} and one Zn^{2+}; thus, the basal inclusions act as inversion domain boundaries (IDB) by flipping the orientation of the ZnO_4 tetrahedra in the adjacent wurtzite region. This structure has recently been confirmed by aberration-corrected TEM.[7,8]

* Address correspondence to p_yang@berkeley.edu.

Received for review July 24, 2013 and accepted November 12, 2013.

Published online November 15, 2013
10.1021/nn403836d

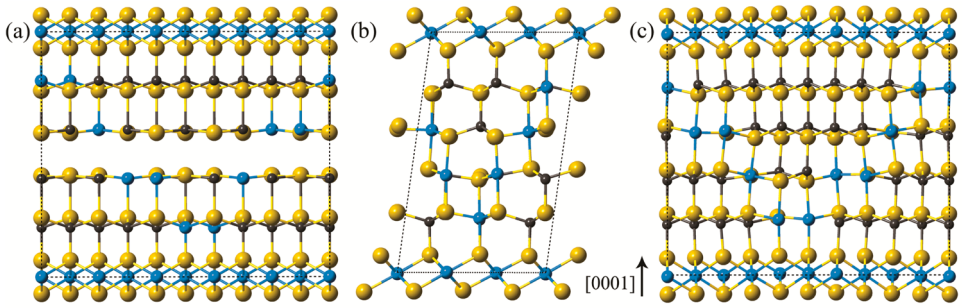

Figure 1. Zigzags in the model proposed by Li *et al.* are shown (a) along the [10$\bar{1}$0] zone axis, with oxygen (yellow), zinc (gray), and indium (blue) atoms. The Yan *et al.* model (b) is viewed along the [11$\bar{2}$0] zone axis. Our proposed structure (c) is more favorable than any alternative model tested. Selected oxygen atoms have been hidden for clarity.

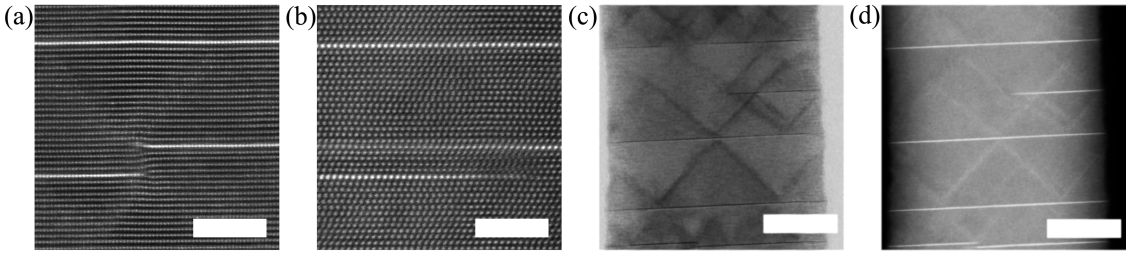

Figure 2. Two basal inclusions meet in the body of an IFZO nanowire, as imaged along the (a) [10$\bar{1}$0] and (b) [11$\bar{2}$0] zone axes (scale bar is 2 nm). Another nanowire segment of IFZO was imaged simultaneously along [10$\bar{1}$0] using (c) bright field and (d) high-angle annular dark field detection (scale bar is 8 nm). See Figure S4 in Supporting Information for greater detail.

Given the constraints on the observed structure, there must be a second IDB in the ZnO to restore the orientation of the tetrahedra between two basal inclusions.[7−9] Additionally, because the charge balance of the crystal is disturbed by the MO_2^- composition of the basal layer, there must be extra M^{3+} ion substitutions to balance the overall charge. Further complexity is presented by the balance between the two alloying metals in indium iron zinc oxide (IFZO). There are a number of competing structural models that attempt to identify the second IDB, as well as the location of the additional M^{3+}, none of which can account for all the experimental observations.

Prior TEM studies of IZO and IFZO revealed a modulated "zigzag" layer in the ZnO slab.[10,11] Li *et al.* suggested that the center of mass in the wurtzite tetrahedra gradually shifts, yielding a trigonal bipyramidal layer in the center of the slab Figure 1a.[12] Here, zigzag contrast is supposedly caused by substitution of M^{3+} for Zn^{2+}, which form $\{1\bar{2}12\}$ planes that are sharply visible along the [10$\bar{1}$0] zone axis. (In this work, we will use the 4 index notation of wurtzite to describe crystal directions, because these are perpendicular to the crystal planes of the same index.) Hörlin *et al.* claimed that the zigzag for IFZO is a $\{1\bar{2}14\}$ plane, based on its incident angle with the basal plane by TEM. They also found that the indium resides predominantly in the basal inclusions, while iron is located mainly in the wurtzite slabs.[11]

More recently, drawing on DFT calculations, Yan *et al.*[13] and Da Silva *et al.*[14] suggested that the IZO zigzags are composed of trigonal bipyramidal indium atoms that serve as the second IDB (Figure 1b). The indium layer is placed on the $\{10\bar{1}1\}$ plane, where it would be sharply visible along [11$\bar{2}$0], contrary to experimental reports.[7−12] Recent calculations using density functional theory (DFT) concluded that the model of Yan *et al.* has a similar formation energy to that of Li *et al.*[15]

RESULTS AND DISCUSSION

The nanowire growth direction is the *c*-axis of wurtzite; therefore, nanowires dispersed on TEM grids were all close to either the [11$\bar{2}$0] or the [10$\bar{1}$0] zone axis, the latter of which is distinguishable by its rectangular pattern of metal atoms. Because the [10$\bar{1}$0] zone axis is 30° around the *c*-axis from the nearest member of the [11$\bar{2}$0] family, it is rare to find a nanowire that allows access to both zone axes within the limited range of the double tilt stage ($\leq$20° for both α and β). The nanowire segment shown in Figure 2 allowed such a rotation, and thus, we could observe the same feature from two directions. This segment contains a pair of edge dislocations that point along the [10$\bar{1}$0] direction, as evidenced by the extra half-plane of Zn atoms at the termination of each basal inclusion. Figure 2a shows zigzag contrast both above and below basal inclusions, where none is visible in Figure 2b on the [11$\bar{2}$0] zone axis. Further observations of defects from two zone axes can be found in the Supporting Information.

IFZO nanowires were imaged simultaneously by bright field and dark field STEM (Figure 2), and contrary to the model of Li *et al.*, the images demonstrate that

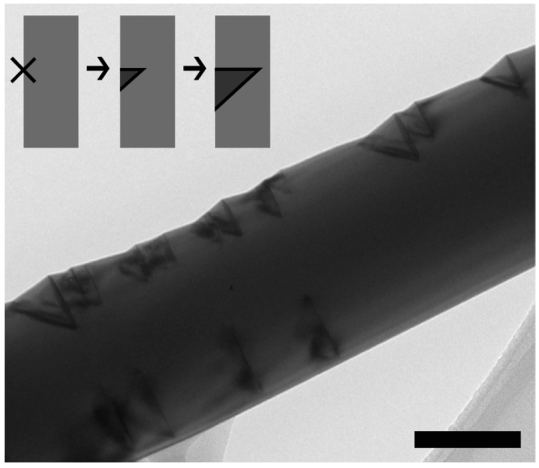

Figure 3. Low magnification TEM of an IZO nanowire formed from attached In_2O_3 nanoparticles shows basal/zigzag inclusion pairs as triangles on the nanowire surface. Scale bar is 100 nm. The cartoon inset depicts conversion of a ZnO nanowire to IZO, beginning from a dislocation formed at the surface (marked by an x). Assuming a plentiful source of In_2O_3, a pair of inclusions (black lines) will grow as the dislocation travels into the body of the nanowire. These inclusions encompass a region of ZnO that has been inverted (shown in dark gray) compared to the original wurtzite orientation of the nanowire.

the second IDB lies along the zigzag itself. The contrast in both images overlaps perfectly, where the dark contrast in bright field shows that the zigzags are regions of strain (as expected for an IDB) while the bright contrast in dark field proves that these same areas are also indium rich. The dual nature of the zigzag as an IDB and site of indium substitution is also shown by DFT calculations of $In_2O_3(ZnO)_3$. For simplicity, we depict the zigzag as a well-defined atomic plane, thus enabling relative comparisons of different single-plane structures (see Supporting Information for further discussion of this approximation). When we use the starting geometry of a *c*-plane IDB in the center of the slab, as in the model of Li *et al.*, the relaxed atomic positions place the IDB along the zigzag itself, by making the indium atoms 5-fold coordinated (Figure 1c). The most stable structure of the type we propose has a total energy per formula unit that is 18 meV lower than that proposed by Yan *et al.*[13] and Da Silva *et al.*[14]

Observation of partially formed IZO wires made from nanoparticle coatings rather than metal films provides further evidence that the zigzag is an IDB. These nanowires were only converted from ZnO locally where nanoparticles attached to the wire surface (Figure 3). Along the length of the nanowire, each basal inclusion is paired with a zigzag. On the basis of this pairing, we deduce that the zigzag is the second IDB and is required for the IZO structure to penetrate the native ZnO.

To assign crystallographic notation to a zigzag plane, we note that it must contain the $[10\bar{1}0]$ vector, so it can be written as $\{1\bar{2}1\ell\}$, where $1/\ell$ is the fractional intersection of the plane with the *c* axis. The angle formed between (0002) and $(1\bar{2}1\ell)$ is the following:

TABLE 1. Calculated energy per formula unit of two crystal compositions over a range of zigzag angles (θ), relative to the most stable zigzag angle for a given composition

ℓ	θ	$In_2O_3(ZnO)_3$	$InFeO_3(ZnO)_3$ (U = 4)
2	58.0°	38 meV	202 meV
3	46.8°	0 meV	31 meV
4	38.7°	18 meV	0 meV
5	32.6°	54 meV	
6	28.1°	83 meV	

$\theta = \tan^{-1}[(2/\ell)\cdot(c/a)]$. The expected angles for a given ℓ value are listed in Table 1, using the c/a ratio of 1.6 for ZnO. The measured zigzag angles for IZO are in the range of 49−59°, so we assign them $\ell = 2-3$.

We find that the zigzag angle depends on the metal composition. A range of 31−48° is observed for samples that contained various proportions of indium and iron, yielding ℓ values of 3−5 for IFZO. DFT total energy calculations of $In_2O_3(ZnO)_3$ and $InFeO_3(ZnO)_3$ confirm this trend (Table 1). In IZO, the most stable computed structure corresponds to $\ell = 3$ (Figure 1c). Calculations of IFZO systems are limited in size to $\ell \leq 4$, due to the added computational expense of spin polarization. Three different values of the effective Hubbard term U_{eff} were applied (3, 4, and 6 eV) with no qualitative change in the results. For all zigzag angles, antiferromagnetic ordering of Fe spins was more stable than ferromagnetic ordering (not shown), in agreement with past literature.[11] We find that in IFZO, the most stable zigzag angle corresponds to $\ell \geq 4$ and is shallower than that of IZO, in agreement with experiment.

EELS data on IFZO further illustrate the dependence of the zigzag angle on the metal composition. Local quantities of iron and indium oxide on the nanowire surface determine the availability of each metal to diffuse and the resulting composition of the inclusions in IFZO, as expressed by the chemical formula $In_{2-x}Fe_xO_3(ZnO)_n$. To identify the relative proportion of In and Fe within either the basal or zigzag layers, EELS line scans were performed across both types of inclusions. Signal from the In $M_{4,5}$ edge was integrated from 481 to 525 eV, and the Fe $L_{2,3}$ edge was integrated from 708 to 743 eV. In Figure 4a, a line scan shows a small Fe concentration across an entire region of IFZO, while the In peak has a sharp increase at the basal inclusion and a small rise at the zigzag. This indicates that the x value for this nanowire segment is low (<1), and indium is the majority M^{3+} ion.

Analysis of another nanowire segment (Figure 4b) shows that the Fe peaks across both types of inclusions are equally strong in this case, and there is no In peak observed in the zigzag. This segment of IFZO therefore has a higher x value than the one shown in Figure 4a, and the angle of this inclusion pair is also noticeably lower (32° *vs* 44°). The distribution of indium and iron between the zigzag and the basal inclusion is likely determined by the stability of the respective ions in

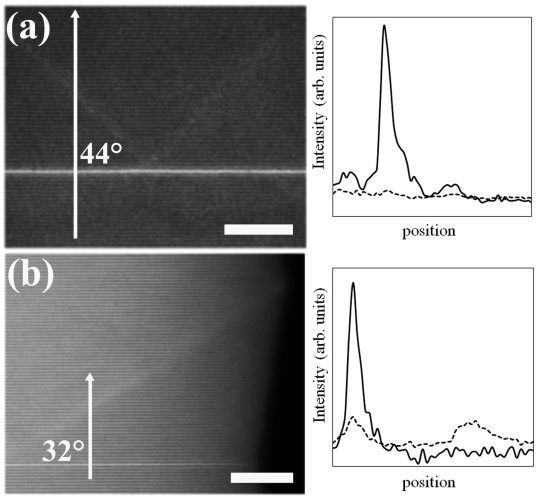

Figure 4. EELS line scans were performed across two areas of an IFZO nanowire, and the integrated peaks of In (solid line) and Fe (dashed line) are plotted in the inset. The zigzag in (a) has a higher incident angle on the basal plane, and shows In in both inclusions and no peak for Fe, while the zigzag in (c) has a lower incident angle and a higher ratio of Fe:In. Scale bar is 5 nm. See Figure S5 in Supporting Information for greater detail.

those coordination environments. The In^{3+} ion is larger than Fe^{3+} (0.80 Å for 6-coordinate In^{3+} *vs* 0.65 for high spin Fe^{3+}).[16] This contributes to the stability of indium in the octahedral site, making the zigzag the preferred site for iron when both species are present.

Taken in total, our data suggest a mechanism for conversion of ZnO to IZO, depicted in Figure 3. During formation of an IZO nanowire, basal inclusion layers move from the surface toward the center as indium diffuses into the ZnO lattice at high temperatures. Because the basal inclusion is an IDB, it must be accompanied by a second IDB during this movement, *i.e.*, the zigzag layer. The IDB requires a transition from tetrahedra through trigonal bipyramids, so there must be a plane of metal atoms with coordination number greater than 4. Indium atoms tend to occupy these sites rather than zinc, because of the +3 charge and the longer In−O bond. The identity of the substituted plane is $\{1\bar{2}1/\}$, where / depends on the metal composition, rather than $\{10\bar{1}1\}$ as in the model of Yan *et al.*

IZO formation is likely initiated by the creation of a misfit dislocation at the interface between ZnO and the indium/iron oxide coating. For the dislocation to move into the nanowire body, it must undergo positive dislocation climb, which occurs by vacancy annihilation.[17] Because indium diffuses into zinc oxide by a vacancy-mediated mechanism,[18] the concentration of zinc vacancies is higher in the nanowire core; therefore, the chemical potential of vacancies in the core of the nanowire is higher than that in the region of the inclusions. This encourages diffusion of vacancies toward the dislocation, facilitating its climb.

Meanwhile, the zigzag follows the edge dislocation into the center of the nanowire, and the M^{3+} cations diffuse to stabilize the zigzag, due to their larger size and preference for larger coordination number compared to Zn^{2+}. Our proposed mechanism assumes that there is a plentiful supply of M^{3+} in the crystal, as well as Zn vacancies in the ZnO lattice. This assumption is valid for IZO at high temperatures, due to the high diffusion constants of both species in ZnO.[18−20] Iron diffusion in ZnO is less well-studied, but is at least somewhat significant at high temperature, as evidenced by iron zinc oxide (FZO) formation.[21]

CONCLUSION

Experimental observations by several groups over two decades are unified under our model of zigzags as $\{1\bar{2}1/\}$ IDBs, based on STEM and EELS analysis of nanowires synthesized by solid state diffusion between ZnO and iron and/or indium oxide coatings. DFT calculations on this structure in IFZO and IZO yield a lower energy than other proposed structures. The zigzag consists of a region of inverting oxygen and zinc layers, around trigonal bipyramidal substitutions of In^{3+} and/or Fe^{3+} in the Zn sites. Zigzags are mobile as basal inclusions and zigzags progress into the nanowire as a pair. This development will enable further optimization and design of these complex oxides.

The validity of our structural model was demonstrated for IZO and IFZO. Further study would entail similarly in-depth imaging and analysis on different alloys in the same crystal family, including quaternary combinations that contain iron, indium and gallium. Though we have described the basal inclusions and the zigzags as planes, the above study does not address the question of their 2D shape (*e.g.*, rectangular, circular, *etc.*). Additional structural data could be collected by X-ray absorption spectroscopy, to obtain a detailed picture of the coordination environment for the various metal sites. Nanowires offer a facile route to TEM sample preparation, but the synthesis of highly uniform samples is limited by the stability of nanoscale morphology; different synthetic techniques could be explored to optimize the phase purity.

METHODS

Nanowire Synthesis. Vertical arrays of ZnO nanowires were grown by a VLS method[22] and then converted to IFZO by previously published methods.[23] Briefly, a ZnO nanowire array was coated with indium and iron by physical deposition methods, including thermal evaporation, and sputtering. No significant difference was observed between samples made by different techniques of metal deposition. Both metal coatings were approximately 10 nm thick as measured by quartz crystal monitor. The array was then exposed to oxygen plasma and annealed for 30 min at 900 °C in an oxygen atmosphere. Due to

the inhomogeneity of the metal deposition, the distributions of indium and iron across the nanowire surface were not equivalent. Each segment along the length of an IFZO nanowire was expected to have a different ratio of indium to iron.

To observe the mechanism of metal diffusion in detail, sparse metal coatings were desired. Indium oxide nanoparticles were synthesized from $In(acac)_3$ in oleylamine, following the procedure of Seo *et al.*,[24] and attached to the ZnO nanowire surface by soaking the array in a dilute solution of particles dispersed in hexanes. The array was then partially converted to IZO at the points of nanoparticle attachment by annealing in oxygen for 30 min at 900 °C. A schematic of both synthetic routes is shown in Figure S3.

Characterization. Arrays of IZO and IFZO nanowires were dispersed on holey carbon support films for electron microscopy. High resolution, aberration-corrected TEM was done on the TEAM 0.5 microscope at the National Center for Electron Microscopy at Lawrence Berkeley National Laboratory (Berkeley, CA). High angle annular dark field (HAADF) scanning transmission electron microscopy (STEM) images and electron energy loss (EELS) data were collected at 300 kV.

Calculations. Density functional theory (DFT) within the generalized gradient approximation (PBE)[25] was used to optimize atomic positions and compute total energies of several IZO and IFZO systems. For all calculations, we used the VASP package[26] and projector augmented-wave potentials.[27] Electrons taken to be valence were In $5s^2 4d^{10} 5p^1$, Fe $3p^6 4s^2 3d^6$, Zn $4s^2 3d^{10}$, and O $2s^2 2p^4$. A plane-wave cutoff of 500 eV was used throughout. In systems with iron, Fe 3d states were treated with an effective Hubbard term $U_{eff} = U - J = 3$, 4, or 6 eV.[28,29] Due to the rapid increase in computational expense with unit cell size, calculations were limited to $In_2O_3(ZnO)_3$ and $InFeO_3(ZnO)_3$. The structure in Figure 1c (110 atoms) is treated with a $5 \times 2 \times 2$ k-point mesh, with k-points for other unit cells scaled accordingly.

Conflict of Interest: The authors declare no competing financial interest.

Acknowledgment. Work performed at NCEM and the Molecular Foundry was supported by the Office of Science, Office of Basic Energy Sciences of the U.S. Department of Energy under Contract No. DE-AC02−05CH11231. V.R.R. also acknowledges supports of Ministry of Education and Science of Republic of Serbia, under contract No. 172054.

Supporting Information Available: Description of the relationship between true zigzag angle and apparent zigzag angle. Additional details on the model for zigzag formation and the synthetic approach. This material is available free of charge *via* the Internet at http://pubs.acs.org.

Note Added after ASAP Publication: This paper was published ASAP on November 15, 2013. Figures 2 and 4 were adjusted for resolution only, and larger versions of the images in F2 (panel c) and F4 (panel a) were added to the end of the previously published Supporting Information. The revised version reposted on November 22, 2013.

REFERENCES AND NOTES

1. Ohta, H.; Seo, W.-S.; Koumoto, K. Thermoelectric Properties of Homologous Compounds in the ZnO-In_2O_3 System. *J. Am. Ceram. Soc.* **1996**, *79*, 2193–2196.
2. Hiramatsu, H.; Seo, W.-S.; Koumoto, K. Electrical and Optical Properties of Radio-Frequency-Sputtered Thin Films of $(ZnO)_5In_2O_3$. *Chem. Mater.* **1998**, *10*, 3033–3039.
3. Nomura, K.; Ohta, H.; Ueda, K.; Kamiya, T.; Hirano, M.; Hosono, H. Thin-Film Transistor Fabricated in Single-Crystalline Transparent Oxide Semiconductor. *Science* **2003**, *300*, 1269–72.
4. Cannard, P. J.; Tilley, R. J. D. New Intergrowth Phases in the ZnO-In_2O_3 System. *J. Solid State Chem.* **1988**, *73*, 418–426.
5. Kimizuka, N.; Mohri, T.; Matsui, Y.; Siratori, K. Homologous Compounds, $InFeO_3(ZnO)_m$ (m = 1−9). *J. Solid State Chem.* **1988**, *74*, 98–109.
6. Kimizuka, N.; Isobe, M.; Nakamura, M. Syntheses and Single-Crystal Data of Homologous Compounds, $In_2O_3(ZnO)_m$ (m = 3, 4, and 5), $InGaO_3(ZnO)_3$, and $Ga_2O_3(ZnO)_m$ (m=7, 8, 9, and 16) in the In_2O_3-$ZnGa_2O_4$-ZnO System. *J. Solid State Chem.* **1995**, *116*, 170–178.
7. Schmid, H.; Okunishi, E.; Mader, W. Defect Structures in ZnO Studied by High-Resolution Structural and Spectroscopic Imaging. *Ultramicroscopy* **2013**, *127*, 76–84.
8. Schmid, H.; Okunishi, E.; Oikawa, T.; Mader, W. Structural and Elemental Analysis of Iron and Indium Doped Zinc Oxide by Spectroscopic Imaging in Cs-Corrected STEM. *Micron* **2012**, *43*, 49–56.
9. Yu, W.; Mader, W. Displacement Field Measurement of Metal Sub-Lattice in Inversion Domains of Indium-Doped Zinc Oxide. *Ultramicroscopy* **2010**, *110*, 411–417.
10. Uchida, N.; Bando, Y.; Nakamura, M.; Kimizuka, N. High-Resolution Electron Microscopy of Homologous Compounds $InFeO_3(ZnO)_m$. *J. Electron Microsc.* **1994**, *43*, 146–150.
11. Hörlin, T.; Svensson, G.; Olsson, E. Extended Defect Structures in Zinc Oxide Doped with Iron and Indium. *J. Mater. Chem.* **1998**, *8*, 2465–2473.
12. Li, C.; Bando, Y.; Nakamura, M.; Onoda, M.; Kimizuka, N. Modulated Structures of Homologous Compounds $InMO_3(ZnO)_m$ (M = In, Ga; m = Integer) Described by Four-Dimensional Superspace Group. *J. Solid State Chem.* **1998**, *139*, 347–355.
13. Yan, Y.; Da Silva, J. L. F.; Wei, S.-H.; Al-Jassim, M. Atomic Structure of In_2O_3−ZnO Systems. *Appl. Phys. Lett.* **2007**, *90*, 261904.
14. Da Silva, J.; Yan, Y.; Wei, S.-H. Rules of Structure Formation for the Homologous $InMO_3(ZnO)_n$ Compounds. *Phys. Rev. Lett.* **2008**, *100*, 255501.
15. Wen, J.; Wu, L.; Zhang, X. A Unique Arrangement of Atoms for the Homologous Compounds $InMO_3(ZnO)_m$ (M = Al, Fe, Ga, and In). *J. Appl. Phys.* **2012**, *111*, 113716.
16. Shannon, R. D. Revised Effective Ionic Radii and Systematic Studies of Interatomic Distances in Halides and Chalcogenides. *Acta Crystallogr.* **1976**, *A32*, 751–767.
17. Hirth, J. P.; Lothe, J. *Theory of Dislocations*; Wiley: New York, 1982.
18. Nakagawa, T.; Matsumoto, K.; Sakaguchi, I.; Uematsu, M.; Haneda, H.; Ohashi, N. Analysis of Indium Diffusion Profiles Based on the Fermi-Level Effect in Single-Crystal Zinc Oxide. *Jpn. J. Appl. Phys.* **2008**, *47*, 7848–7850.
19. Erhart, P.; Albe, K. Diffusion of Zinc Vacancies and Interstitials in Zinc Oxide. *Appl. Phys. Lett.* **2006**, *88*, 201918.
20. Tomlins, G. W.; Routbort, J. L.; Mason, T. O. Zinc Self-Diffusion, Electrical Properties, and Defect Structure of Undoped, Single Crystal Zinc Oxide. *J. Appl. Phys.* **2000**, *87*, 117–123.
21. Li, C.; Bando, Y.; Nakamura, M.; Kimizuka, N. Antiphase Modulated Structure of $Fe_2O_3(ZnO)_{15}$ Studied by High-Resolution Electron Microscopy. *J. Solid State Chem.* **1999**, *142*, 174–179.
22. Huang, M. H.; Mao, S.; Feick, H.; Yan, H.; Wu, Y.; Kind, H.; Weber, E.; Russo, R.; Yang, P. Room-Temperature Ultraviolet Nanowire Nanolasers. *Science* **2001**, *292*, 1897–1899.
23. Andrews, S. C.; Fardy, M. A.; Moore, M. C.; Aloni, S.; Zhang, M.; Radmilovic, V.; Yang, P. Atomic-Level Control of the Thermoelectric Properties in Polytypoid Nanowires. *Chem. Sci.* **2011**, *2*, 706–714.
24. Seo, W.-S.; Jo, H. H.; Lee, K.; Park, J. T. Preparation and Optical Properties of Highly Crystalline, Colloidal, and Size-Controlled Indium Oxide Nanoparticles. *Adv. Mater.* **2003**, *15*, 795–797.
25. Perdew, J.; Burke, K.; Ernzerhof, M. Generalized Gradient Approximation Made Simple. *Phys. Rev. Lett.* **1996**, *77*, 3865–3868.
26. Kresse, G.; Furthmüller, J. Efficient Iterative Schemes for *ab Initio* Total-Energy Calculations Using a Plane-Wave Basis Set. *Phys. Rev. B* **1996**, *54*, 11169–11186.
27. Kresse, G.; Joubert, D. From Ultrasoft Pseudopotentials to the Projector Augmented-Wave Method. *Phys. Rev. B* **1999**, *59*, 1758–1775.
28. Dudarev, S. L.; Botton, G. A.; Savrasov, S. Y.; Humphreys, C. J.; Sutton, A. P. Electron-Energy-Loss Spectra and the Structural Stability of Nickel Oxide: An LSDA+U Study. *Phys. Rev. B* **1998**, *57*, 1505–1509.
29. Wang, L.; Maxisch, T.; Ceder, G. Oxidation Energies of Transition Metal Oxides Within the GGA+U Framework. *Phys. Rev. B* **2006**, *73*, 195107.